Desalination and Water Treatment
www.deswater.com

doi: 10.5004/dwt.2023.29545

297 (2023) 75–87
June

Preparation of activated carbon-based composite adsorbent and its efficient adsorption of Cr(VI) from aqueous solution

Yarui Song[†], Zhaoxi Du[†], Kaisheng Wang, Fajun Zhao*

Ministry of Education Key Enhanced Oil and Gas Recovery Laboratory, Northeast Petroleum University, Daqing, China, emails: fajzhao@126.com (F.-j. Zhao), songyr2003@163.com (Y.-r. Song), dyduzhaoxi@163.com (Z.-x. Du), 18814592817@163.com (K.-s. Wang)

Received 26 September 2022; Accepted 5 April 2023

ABSTRACT

In current work, using powdered activated carbon, potassium humate, and polyaluminium chloride as raw materials, we have generated the new powdered activated carbon-based composite (PACMC). Scanning electron microscopy-energy-dispersive X-ray spectrometry, Fourier-transform infrared spectrometer, laser particle size analyzer and zero point charge analyses were used to characterize the PACMC. The prepared PACMC were tested for the removal of Cr(VI) at different pH, initial metal ions concentration, adsorbent dosage, time, and temperature. The results demonstrated that PACMC led to the removal efficiency of Cr(VI) being 95.67% at pH 2.0, with the equilibrium adsorption capacity of 23.92 mg/g (dosage = 2 g/L, C_0 = 50 mg/L). The kinetic studies indicated that pseudo-second-order and Elovich models fit the experimental data well. The Temkin model gives the best fit for the adsorption of Cr(VI). Moreover, thermodynamic parameters revealed that the adsorption of Cr(VI) on PACMC was an endothermic and spontaneous process. Importantly, the binding mechanism of Cr(VI) is primarily controlled by the electrostatic attraction between Cr(VI) and the protonated functional groups of PACMC. Reducing functional groups (such as carboxyl, hydroxyl, carbonyl) in PACMC can be used as electron donors, and Cr(VI) has strong oxidation, so Cr(VI) can be reduced to Cr(III). Overall, PACMC served as a potential adsorbent to remove harmful Cr(VI) from aqueous solution.

Keywords: Hexavalent chromium; Adsorption; Powder activated carbon; Process capability study

1. Introduction

Industrial development has brought great economic benefits, but it has also caused great harm to the water environment. In particular, industrial wastewater contains a large number of heavy metal ion pollutants. Trace heavy metal concentrations can trigger ecological imbalances due to their toxicological and physiological effects on the environment. Cr(VI) is widely used in printing and dyeing, metal processing, electroplating, nuclear power, tanning, photography, textile and other industries [1]. Cr(VI) has strong oxidizing, highly toxic and non-biodegradable properties [2–4], and it is easy to migrate in water, which leads to the expansion of pollution scope. If it is not discharged properly, it will pose a serious threat to the ecosystem. Cr(VI) is mutagenic, carcinogenic and teratogenic [5,6], and also has high solubility, mobility, bioaccumulation and diffusion across cell membranes [7]. It also can lead to DNA damage, cell death, liver and kidney dysfunction in humans [8,9]. The World Health Organization lists Cr(VI) as the second largest inorganic groundwater contaminant [10]. According to the regulations of the World Health Organization (WHO), the maximum allowable concentration of Cr(VI) in industrial wastewater released into surface water is 0.1 mg/L, and

---

* Corresponding author.
[†] Both authors contributed equally to this work.

1944-3994/1944-3986

the allowable maximum concentration in drinking water is 0.05 mg/L [11]. Therefore, the removal of Cr(VI) from water is an extremely important environmental challenge.

There are several treatment methods available to remove Cr(VI) from wastewater, such as chemical precipitation [12], membrane treatment [13], electrodialysis, biological reduction [14], ion-exchange [15,16], photocatalysis method [17,18] and adsorption method [1]. However, considering the impact of high energy requirements, complex processes or the generation of toxic by-products, many technologies are limited to varying degrees in practical applications. Among them, adsorption has been widely used for its advantages of simple operation, flexible design, economy, high efficiency and applicability to different effluent conditions [5]. The key to adsorption method is the selection of a suitable adsorbent for the target pollutant [16]. Practical adsorbent materials are usually inexpensive, readily available, efficient and can be adapted to specific needs (such as facilitating the resource utilization of pollutants, easy recovery, easy separation and regeneration). The oldest and most widely used adsorbent in the water treatment industry is activated carbon [19]. With its huge specific surface area, superior pore structure and high stability, activated carbon has the potential for sustainable development in the water treatment industry [20,21]. Powdered activated carbon (PAC) is valued for its low-cost, high efficiency and environmental friendliness. The adsorption capacity of PAC increases significantly when its particle size is reduced from tens of microns to a few microns [22], but it needs to increase the additional processes for removing PAC particles after removing pollutants, such as coagulation. In addition, while PAC has good adsorption capacity for hydrophobic compounds, it has moderate adsorption efficiency for hydrophilic compounds. Adsorbent performance has been reported to be limited by the major functional groups on the surface and within the pores, therefore, re-functionalisation of existing adsorbents has become a new mega trend [1]. Modification of activated carbon, such as loading or doping of other functional substances on its surface, is an effective way to enhance and optimise the performance of activated carbon. For example, coating nano-α-FeOOH on activated carbon by impregnation method can significantly improve the removal of Cr(VI) [23]. Immobilising nZVI particles on activated carbon can improve adsorption capacity of Cr(VI) and be regenerate [24]. Based on this, this paper intends to search for new, innovative and cost-effective activated carbon-based composites for efficient Cr(VI) adsorption and removal. At the same time, the activated carbon-based composites should reach the balance between the contaminant removal and the clarification performance for efficient treatment.

Therefore, it is the aim of this work to prepare powdered activated carbon-based composite materials (PACMC) for very efficient Cr(VI) adsorption from aqueous solution with a much better adsorption and separation performance. In this paper, activated carbon-based adsorbent materials (PACMC) were constructed by introducing potassium humate (HS) and polyaluminium chloride (PACl) on the basis of PAC. The physicochemical properties of PACMC were characterised by scanning electron microscopy-energy-dispersive X-ray spectrometry (SEM-EDS), Fourier-transform infrared spectrometer (FTIR) and surface charge analysis. Batch experiments were carried out under different physicochemical conditions (initial Cr(VI) concentration, adsorbent dosage, initial pH, adsorption time and temperature), and the adsorption isotherms, kinetic and thermodynamic models were equipped with the experimental results to investigate the adsorption performance and adsorption mechanism of PACMC on Cr(VI), which are of significance for understanding the process and mechanism of adsorption materials.

2. Materials and methods

2.1. Materials

HS with a purity of 98%, was purchased from Beijing Bowei Shennong Technology Co., Ltd., (China). PACl with alkalinity (OH/Al) of 1.35, Al_2O_3 content of 30% (wt.), was purchased from Nanning Chemical Co., Ltd., (China). Powdered activated carbon, was purchased from Xilong Science and Chemical Co., Ltd., (China). Potassium dichromate ($K_2Cr_2O_7$), was purchased from Tianjin Kemeiou Chemical Reagent Co., Ltd., (China). All of the materials were of analytical grade. During the experiments, all solutions were manufactured with deionized water.

2.2. Preparation of PACMC composites

Accurately weighed 4.42 g of HS, PACl and PAC (mass ratio 1:1:1), and three materials were made into a composite material according to the following steps. First, HS and PAC were added to 500 mL of 40°C deionised water and stirred for 20 s. Then PACl was added and whisked for 20 s. The resulting suspension was shaken at ambient temperature for 12 h. The precipitation was left to stand and the solid–liquid was separated. The supernatant solution was discarded, and the solids was dried at 80°C. The dried sample was ground using a mortar and pestle and characterized.

2.3. Characterization of PACMC composite

Sample morphology and element mapping were observed using a scanning electron microscopy-energy-dispersive X-ray spectrometer (SEM-EDS, GEMI NISEM 500, GER). The functional groups on the surface of each sample were analyzed by (FTIR, Nicolet iS50, USA).

Determination of the point of zero charge (pH_{PZC}) is essential for a clearer understanding of the surface properties of the adsorbent during the adsorption process. The point of zero charge of PACMC composites determined by zeta potential measurements [25].

The zeta potential was performed using Zetasizer (Malvern, UK). Disperse PACMC particles in water at a concentration of 200 mg/L, the suspensions adjusted for the desired pH (in the range 2–9) and sedimented/conditioned for 2 h at 25°C in 250 mL conic flasks containing potassium nitrate solution (0.03 mol/L) as an indifferent electrolyte. The applied tension varied between 75 and 200 mV. The zeta potentials of PACMC was expressed as the average values from 10 repetitions.

2.4. Adsorption experiments

Potassium dichromate was used to prepare Cr(VI) stock solution with Cr(VI) concentration of 1,000 $mg\cdot L^{-1}$, which was diluted and used according to demand in subsequent experiments. All batch adsorption experiments were performed in a constant temperature oscillation incubator to ensure good mixing, and the vibration speed was 120 rpm. Three replicates for each experimental combination were performed to investigate the effects of parameters like pH value, adsorbent dosage, initial metal ion concentration, and contact time effect on Cr(VI) removal. The solution pH was adjusted by 0.1 M NaOH and 0.1 M HCl. After the experiments the solution was filtered by 0.45 μm filter membrane and a UV-Vis spectrophotometer (TU-1810) was used to specify the concentration of a solution by measuring its absorbance value at λ = 440 nm. The adsorption capacity q_e ($mg\cdot g^{-1}$) of the adsorbed heavy metal ions was calculated according to Eq. (1) [26]:

$$q_e = \frac{V\left(C_o - C_e\right)}{W} \quad (1)$$

where C_0 and C_e are the initial and equilibrium metal ion concentrations ($mg\cdot L^{-1}$), respectively, V (L) is the volume of the solution, and W (g) is the mass of the adsorbent.

Calculation of metal ion removal ($R\%$) was estimated from Eq. (2) [26]:

$$R\% = \frac{\left(C_0 - C_e\right)}{C_0} \times 100 \quad (2)$$

where C_0 ($mg\cdot L^{-1}$) is the initial concentration of metal ions in the solution, and C_e ($mg\cdot L^{-1}$) is the equilibrium concentration of metal ions.

2.5. Adsorption kinetics

Adsorption kinetics is a key technique for determining the mechanism controlling adsorption and describing the adsorption rate, depending on the physicochemical properties and mass transfer processes between the adsorbent and the adsorbate. The pseudo-first-order kinetic model, pseudo-second-order kinetic model, Elovich model, and intraparticle diffusion model were used to study the adsorption process of Cr(VI), and they were expressed by Eqs. (3)–(6) [27–29]:

$$Q_t = Q_e\left(1 - \exp\left(-k_1 t\right)\right) \quad (3)$$

$$Q_t = \frac{Q_e^2 k_2 t}{1 + Q_e k_2 t} \quad (4)$$

$$Q_t = \alpha + \beta \ln t \quad (5)$$

$$Q_t = k_d t^{1/2} + C \quad (6)$$

where Q_t and Q_e are the adsorption capacities of Cr(VI) at time t and at equilibrium ($mg\cdot g^{-1}$), respectively; k_1 (min^{-1}) and k_2 ($g\cdot mg^{-1}\cdot min^{-1}$) are the equilibrium rate constants for pseudo-first-order and pseudo-second-order models, respectively; α ($mg\cdot g^{-1}\cdot min^{-1}$) and β ($g\cdot mg^{-1}$) are the Elovich constants; k_d is the intraparticle diffusion coefficient ($mg\cdot g^{-1}\cdot min^{-1}$); C is the intercept of the line, related to the thickness of the boundary layer.

2.6. Adsorption isotherms

The isotherm represents adsorption equilibrium, that is, the ratio of adsorbed volume to equilibrium concentration or pressure at constant temperature [30]. Isotherms indicate the retention mechanism of the solution component and solid-phase in equilibrium as well as the surface properties and affinity of the adsorbent, which are important in the interpretation of the adsorption process sufficiently [31]. In order to analyse the adsorption behaviour of PACMC for Cr(VI), the experimental data were modeled using Langmuir, Freundlich and Temkin isotherm adsorption models, which were expressed in the following form [32,33]:

$$Q_e = \frac{Q_{\max} K_L C_e}{1 + K_L C_e} \quad (7)$$

$$Q_e = K_F C_e^{1/n} \quad (8)$$

$$Q_e = B \ln K_T + B \ln C_e \quad (9)$$

where Q_e is the adsorption capacity at equilibrium ($mg\cdot g^{-1}$); C_e is the adsorbate concentration at equilibrium ($mg\cdot L^{-1}$); $Q_{\max}$ is the maximum adsorption capacity ($mg\cdot g^{-1}$); K_L, K_F and K_T are the adsorption equilibrium constants for the Langmuir, Freundlich and Temkin isotherm equations; n is a non-uniformity-dependent constant.

2.7. Adsorption thermodynamics

Through thermodynamic research, the direction and degree of reaction of a physicochemical process can be determined. The van't Hoff equation is used to explore the properties of the adsorption process and the relevant parameters, such as standard enthalpy ($\Delta H°$), standard entropy ($\Delta S°$) and the change in standard Gibbs free energy ($\Delta G°$) were calculated by Eqs. (10) and (12) [7,27,34]:

$$\Delta G° = -RT \ln K_d \quad (10)$$

$$\ln K_d = \frac{\Delta S°}{R} - \frac{\Delta H°}{RT} \quad (11)$$

$$\Delta G° = \Delta H - T\Delta S \quad (12)$$

where K_d (dimensionless) is the thermodynamic equilibrium constant, $K_d = Q_e/C_e$, Q_e is the adsorption capacity at equilibrium ($mg\cdot g^{-1}$), C_e is the adsorbate concentration at equilibrium ($mg\cdot L^{-1}$); R is the universal gas constant (8.314 $J\cdot mol^{-1}\cdot K^{-1}$) and T is the absolute temperature (K).

3. Results and discussions

3.1. Characterization

The morphology of the adsorbent material is an important aspect in the analysis of the adsorption process. The diffusion and deposition of heavy metal ions in the pores of the adsorbent material will be affected by the pore structure and distribution. The SEM morphologies of PAC and PACMC are shown in Fig. 1. As shown in Fig. 1D, the surface of PAC is uneven and has a relatively rich pore structure. The PACMC particles have irregular morphology with fractured and rough surfaces, and there are a large number of non-uniform pores (Fig. 1E and F. HS and PACl are successfully deposited on the surface and within the pore channels of PAC, which facilitates the diffusion of contaminants into the interior of the PACMC material. Therefore, PACMC can be used as an effective adsorbent for wastewater purification. The SEM of PACMC after adsorption are given in Fig. 1G–I. Basically, the uneven structure that appears in Fig. 1E gets disorder in Fig. 1G–I because of adsorption.

Fig. 4a shows the FTIR spectrum. After PACMC synthesis, it can be observed that the major changes of PACMC infrared spectra occur in the region 3,700–1,000 cm^{-1}, in which the adsorption bands of oxo-groups or bridges appear. Specifically, in the PACl and HS spectra, the band at 3,400 cm^{-1} gradually degenerates into three distinct bands at 3,669; 2,990 and 2,898 cm^{-1}. In this region, bands related with the vibrations of C–C bonds appear. After the PAC and HS addition, the band at 1,105 cm^{-1} in the PACl spectra progressively degenerates into two distinct bands at 1,065 and 1,255 cm^{-1}. The shift of those bands at lower wavelengths in PACMC indicates a possible weakening of their strength. In the case of HS, the peaks at 3,150 and 1,572 cm^{-1} correspond to O–H stretching vibrations and C=O stretching vibrations in carboxylic acids; the absorption bands at 1,095 and 1,370 cm^{-1} are attributed to C–O stretching and O–H bending vibrations in phenols or alcohols, respectively [35]. In the case of PAC, the absorption peak at 1,142 cm^{-1} corresponds to the stretching vibration of phenolic or alcohol C–O; the stretching vibration of C=O in the presence of carboxylic acids is associated with the absorption peak at 1,570 cm^{-1} [36,37]. In the case of PACl, and the absorption peak at 3,024 cm^{-1} corresponds to the stretching vibration of O–H [38]. The alteration of bands indicates that PACl, PAC and HS molecules are all affected by the combination of three compounds. Furthermore, at the region 1,000–600 cm^{-1}, the two weak bands appearing in the PACl spectra gradually disappear; and at the region 1,700–1,400 cm^{-1} the three weak bands appearing in the PACl, PAC and HS spectra gradually disappear. These bands are associated with oxo-groups or oxo-bridges vibrations, and the disappearance might be an indication of interaction among PACl, PAC and HS molecules. Summarizing, the introduction of PACl and PAC results in significant alterations in the infrared spectra of the system. These variations could be ended up causing by interactions among PACl, PAC and HS molecules, such as covalent bonding and electro-static interactions, which lead to the formation of new, composite species. The carboxyl and hydroxyl groups on HS, the hydroxyl groups on PACl, and the carboxyl and hydroxyl groups on PAC can all participate in the interaction through covalent bonds [39]. The carboxyl and hydroxyl functional groups on HS can also interact with the carboxyl and hydroxyl groups on PAC through hydrogen bonding, enhancing their affinity for one another [40]. At the same time, as shown in Fig. 2, compared with PAC, the content of carbon element in PACMC is reduced, and the content of oxygen element is increased, which indicates that –OH and –COOH are introduced into PACMC. The preparation route and microstructure schematic diagram of PACMC are speculated as shown in Fig. 3. It is speculated that PAC and HS are the main reaction bodies in the process of synthesizing PACMC, and PACl acts as a binder through coagulation. PAC plays the role of providing channels and a high surface area, providing sites for the implantation of functional groups of HS. PACl organically binds HS to the surface of PAC through bridging, providing functional groups that can have strong interaction with heavy metal

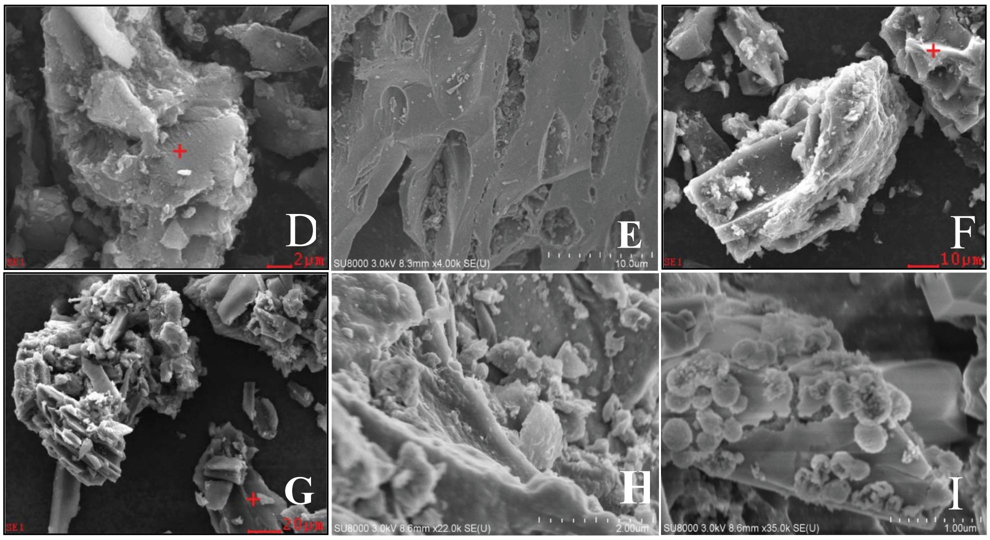

Fig. 1. Scanning electron microscopy images of (D) PAC, (E,F) PACMC and (G–I) PACMC after Cr(VI) adsorption.

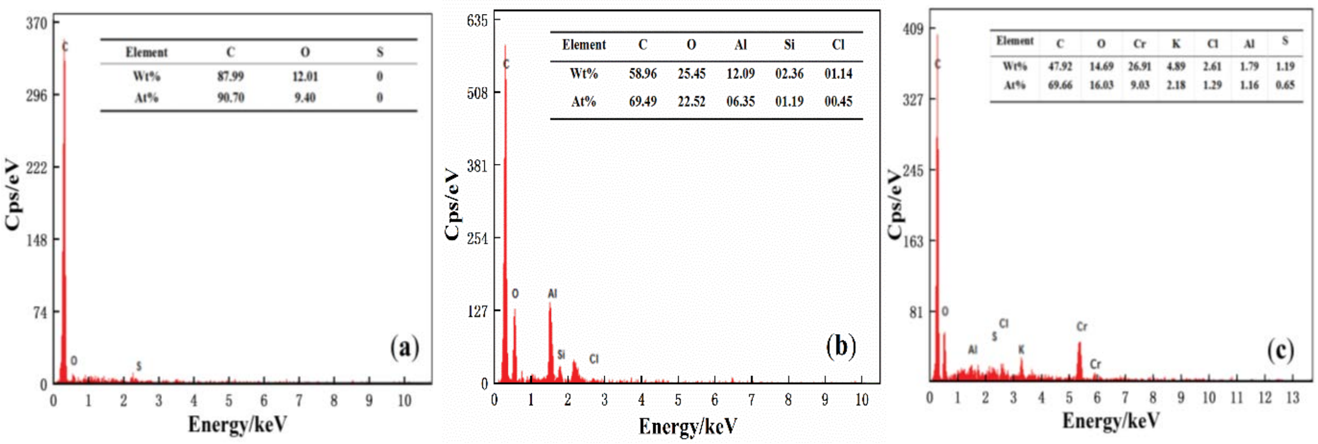

Element	C	O	S
Wt%	87.99	12.01	0
At%	90.70	9.40	0

Element	C	O	Al	Si	Cl
Wt%	58.96	25.45	12.09	02.36	01.14
At%	69.49	22.52	06.35	01.19	00.45

Element	C	O	Cr	K	Cl	Al	S
Wt%	47.92	14.69	26.91	4.89	2.61	1.79	1.19
At%	69.66	16.03	9.03	2.18	1.29	1.16	0.65

Fig. 2. EDS elemental of (a) PAC, (b) PACMC and (c) PACMC after Cr(VI) adsorption.

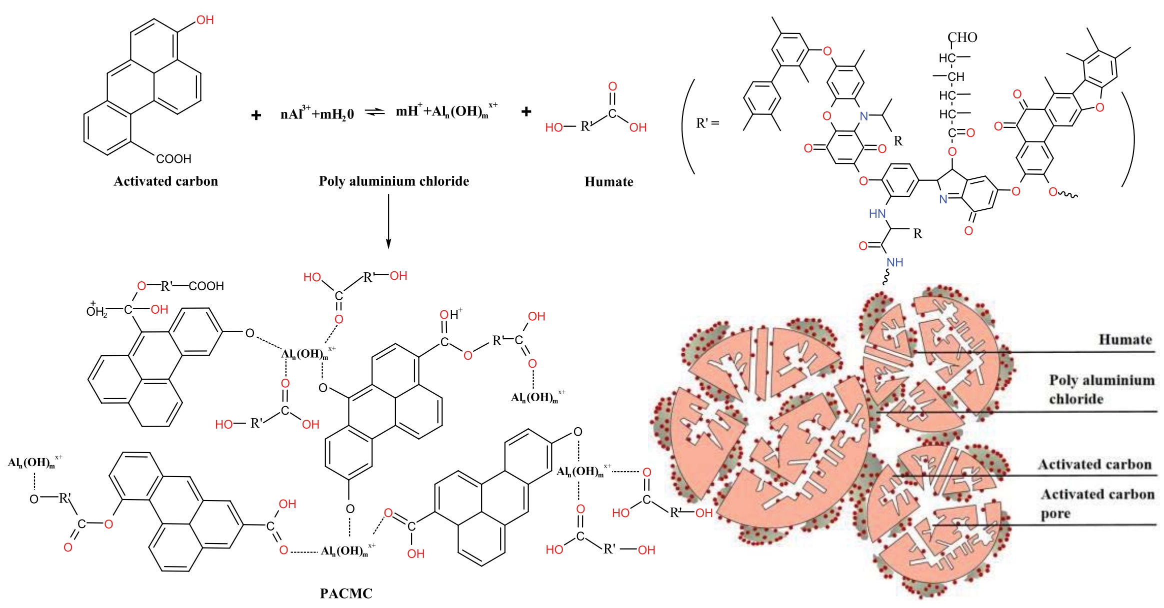

Fig. 3. Microstructure and preparation reaction roadmap of PACMC.

ions. In the meantime, the bridging effect makes the bond between PAC, HS and PACl stronger, which enhances the solid–liquid separation potential of the adsorbent and the efficiency of recycling.

The energy spectra of PAC and PACMC are shown in Fig. 2a and b. The EDS spectra indicate the presence of C, O and Al elements indicating that HS, PACl and PAC have been successfully compounded. The composition of PACMC is high in both carbon and oxygen, which are the main components of PAC and HS. By comparing Fig. 2b and c, it can be seen that silicon do not appear on all surfaces, which indicates that PAC and HS are unevenly distributed in the preparation process of PACMC.

The EDS spectrum of the hybrid composites after the removal of Cr(VI) by PACMC is shown in Fig. 2c. The results show that Cr element is detected in the mixed material. EDS spectra showed that new peaks appeared at 5.4 and 5.9 keV after the adsorption of Cr(VI) on the surface of PACMC, further confirming the successful adsorption of Cr(VI) onto the surface of PACMC.

The specific surface area (10.098 $m^2 \cdot g^{-1}$) and average particle size (147.2 μm) of PACMC were measured experimentally. At the same time, the specific surface area (710.1 $m^2 \cdot g^{-1}$) and average particle size (11.9 μm) of PAC were measured. By comparison, it is found that PACMC has a relatively small specific surface area and greater average particle size. Specific surface area and chemical properties are two important factors in determining the adsorption capacity of an adsorbent. The introduction of HS and PACl makes the specific surface area of PACMC smaller than that of PAC, but it also introduces a significant amount of active functional groups (–OH, –COOH) to the adsorbent's surface, increasing its affinity for Cr(VI). Fig. 4b depicts the corresponding histogram of particle-size distribution, the particle-size distribution of PACMC is wider, in the range of tens of micrometers to hundreds of micrometers, compared with

PAC alone, it can achieve better solid–liquid separation and recycling.

3.2. Cr(VI) adsorption performance

3.2.1. Adsorption performance comparison of Cr(VI)

As given in Fig. 5a, the effectiveness on the elimination of Cr(VI) from aqueous solutions using PAC, PACl and PACMC adsorbent was investigated within different Cr(VI) initial concentrations. In the initial Cr(VI) range of 20–100 mg·L^{-1}, the adsorption effect of PACMC is better than that of PACl and PAC. PACMC could remove 94.76% and 94.13% of Cr(VI) at initial Cr(VI) concentrations of 20 and 40 mg·L^{-1}, respectively, whereas PACl and PAC only eliminated 56.88%/44.98% at Cr(VI) concentrations of 20 mg·L^{-1}, and 54.23%/41.65% at Cr(VI) concentrations of 40 mg·L^{-1}, respectively. This indicated that PACMC was more suitable for adsorption treatment of Cr(VI) wastewater. It can be attributed to the fact that HS is rich in a large number of active functional groups, and the introduction of HS

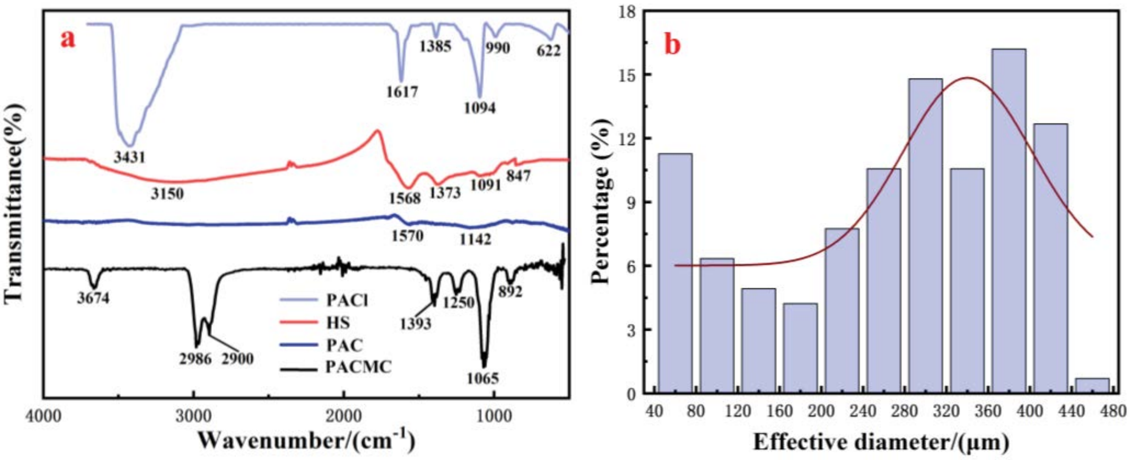

Fig. 4. (a) Fourier-transform infrared spectra of composites and each single-component and (b) particle-size distribution of PACMC.

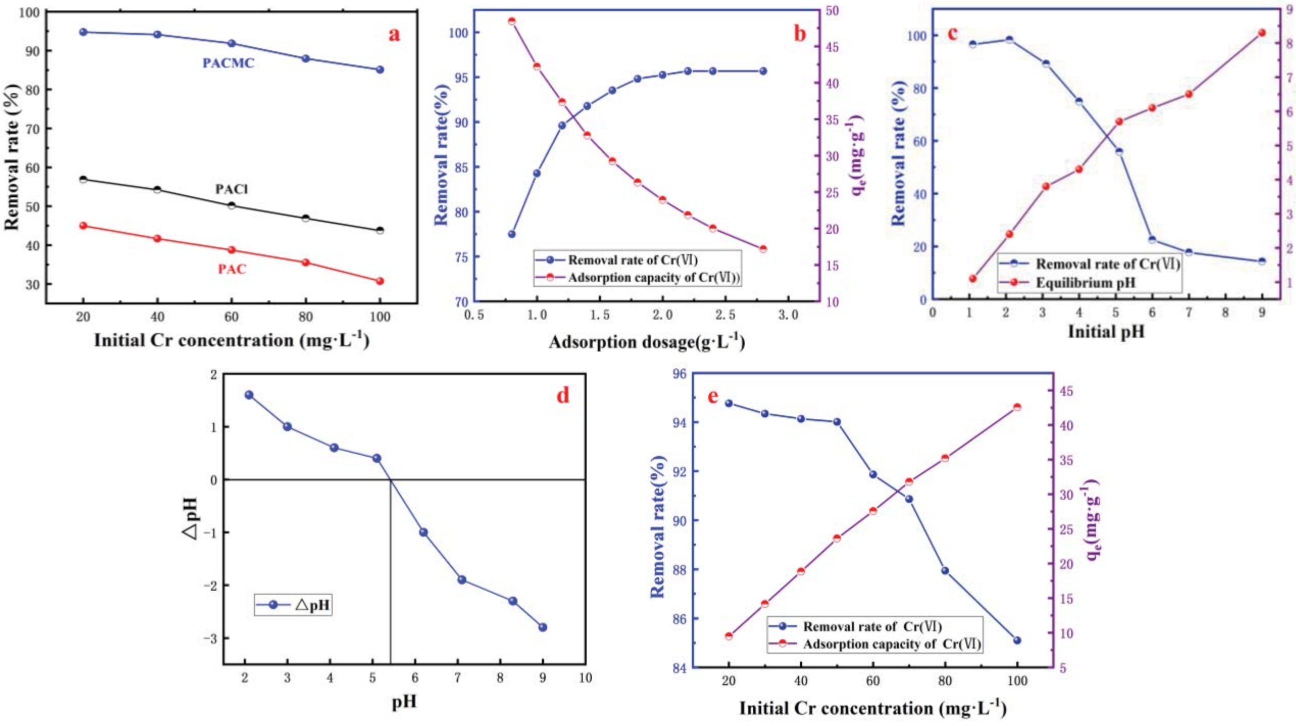

Fig. 5. (a) Comparison of Cr(VI) adsorption performance between PACMC, PACl and PAC, (b) effect of PACMC dosage on Cr(VI) adsorption, (c) effect of initial pH on Cr(VI) adsorption by PACMC, (d) point of zero charge analysis of PACMC and (e) effect of initial Cr(VI) concentration on Cr(VI) adsorption by PACMC.

increases the active adsorption sites of PACMC, which aided in the improvement in the adsorption capacity of PACMC.

3.2.2. Effects of adsorbent dosage

The removal performance of Cr(VI) was investigated by varying the dosage of PACMC from 0.8 to 2.8 g·L^{-1}. Fig. 5b shows that the removal efficiency varies with the dosage of PACMC. Two scenarios (growth and equilibrium) of Cr(VI) ion adsorption rates were observed with increasing adsorbent dosage, the gradual increase in adsorption rate was mainly due to an increase in the number of active binding sites and more collisions of Cr(VI) with the adsorbent [41,42]. When the adsorbent dosage was increased from 0.8 to 2.0 g·L^{-1}, the amount of Cr(VI) adsorbed by PACMC decreased from 48.43 to 23.92 mg·g^{-1}, and the removal efficiency of Cr(VI) was significantly increased from 77.49% to 95.24%. The adsorption efficiency remained essentially stable when the dosage of PACMC composites exceeded 2.0 g·L^{-1}. This observation was due to the competitive adsorption among the adsorbents at higher adsorbent dosages, leading to the unsaturation of the adsorption sites.

3.2.3. Effect of solution pH

The pH value influences the surface charge on the adsorbent and the speciation of heavy metal ions in the solution, and is a crucial parameter for evaluating the mechanism of metal ion removal [4,43]. In this study, the adsorption of Cr(VI) by the adsorbent material was investigated at various pH values ranging from 1 to 7. Fig. 5c demonstrates that the PACMC adsorption capacity for Cr(VI) was higher at pH ≤ 2 and thereafter it decreased significantly with increasing pH. And it can be seen that the maximal adsorption capacity of PACMC for Cr(VI) reached a maximum value of 23.92 mg·g^{-1} at pH = 2, with a significant Cr(VI) removal rate of 95.67%. When pH = 9, the adsorption effect was the worst, and the Cr(VI) removal rate was only 14.29%. The main reason for this is that the pH of the solution influences the form of Cr(VI) in aqueous solution and there are several types of $HCrO_4^-$, $Cr_2O_7^{2-}$ and CrO_4^{2-} [44,45]. In the pH = 2–6 range, Cr(VI) is present in the environment is in the form of $HCrO_4^-$ and $Cr_2O_7^{2-}$. When pH > 6.0, the most abundant form of Cr(VI) is CrO_4^{2-} [4]. From Fig. 5d, the PZC value of the PACMC was determined to be 5.4. The active sites of PACMC are mainly hydroxyl and carboxyl groups. When the pH value was low (<pH_{PZC}), the surface functional groups of PACMC were protonated ($-OH_2^+$ and $-COOH_2^+$) and attracted Cr(VI) anions ($HCrO_4^-$ and $Cr_2O_7^{2-}$), improving the removal rate of Cr(VI). Conversely, as the pH increased, the negatively charged active sites on the surface of PACMC increased, and there was a significant electrostatic repulsion between PACMC and Cr(VI) anions, which limited the binding of Cr(VI) on PACMC, resulting in a reduction in Cr(VI) ion adsorption rate with the increase of pH. Therefore, pH = 2 was the optimum pH value for conducting subsequent adsorption experiments.

3.2.4. Effect of initial concentration

The impact of PACMC dosage mostly on adsorption capacity and removal efficiency of Cr(VI) ions was evaluated at Cr(VI) ion concentrations ranging from 20 to 100 mg·L^{-1}. As can be seen from Fig. 5e, as the adsorbent concentration rose from 20 to 100 mg·L^{-1}, the equilibrium amount of Cr(VI) removed increased from 9.48 to 42.55 mg·g^{-1} ,whereas removal efficiency dropped from 94.76% to 85.10%. The initial concentration of Cr(VI) enhanced the amount of chromium ions absorbed for each unit mass of adsorbent. This phenomenon was attributed to the higher initial ion concentration providing the necessary driving power to overcome the resistance to metal ion mass transfer between the solid and aqueous phases, along with the increased collision rate between the adsorbent and adsorbate [21]. The decrease in removal efficiency with increasing chromium ion concentration was probably due to the saturation of the active binding site at higher concentrations and the increased amount of unsorbed chromium ions in solution. The above researches show that PACMC composites can more effectively remove Cr(VI) than powdered activated carbon in aqueous solution. This phenomenon is mainly due to the large number of active groups in PACMC, which creates many different potential sites for metal ion binding. Furthermore, the relatively large particle size of PACMC makes it simple to separate the adsorbent from water after the adsorption process.

3.3. Adsorption kinetics

At an initial mass concentration of 100 mg·L^{-1}, the influence of contact time on the removal of Cr(VI) in the presence of PACMC composites was investigated (Fig. 6a). The results showed an increase of the Cr(VI) adsorption as increasing the contact time. However, a fast Cr(VI) adsorption was observed up to 60 min. Then it became slower until to reach a maximum value of 95.02% at 420 min with the Cr(VI) adsorption of 23.755 mg·g^{-1}. The rapid increase in adsorption during the first period was due to the presence of a large number of effective adsorption sites on the PACMC surface, and the solid–liquid interface of the adsorbent–adsorbate contained a large amount of Cr(VI). As the number of empty binding sites decreased as contact time increased, and electrostatic repulsion was generated between the residual Cr(VI) ions in the solution and the Cr(VI) ions previously adsorbed onto the surface of the PACMC composite, resulting in a slower adsorption rate and gradually reach equilibrium.

The kinetics of Cr(VI) on PACMC fit the pseudo-second-order and Elovich models. Fig. 6a shows the fitted curves for the pseudo-first-order, pseudo-second-order and Elovich models and the kinetic parameters are shown in Table 1. Due to the inhomogeneous distribution of chemical bonds in PACMC, several models have shown good compatibility with experimental data. Table 1 demonstrates that the R^2 (0.9995) of the pseudo-second-order equation is slightly larger than the R^2 (0.9986) of the pseudo-first-order equation, indicating that the pseudo-secondary equation is more suitable for describing the adsorption process, and it also shows that both physical (pore filling and electrostatic adsorption) and chemical (electron transfer) effects may exist for the adsorption of Cr(VI) by PACMC. In addition, the experimental values ($Q_{e,\mathrm{exp}}$) for Cr(VI) adsorption by PACMC are close to the calculated values, indicating that the data fits the model effectively. The Elovich kinetic model is related to chemisorption and is usually adapted to systems where the adsorbent has a non-homogeneous surface [46]. The fitted curve of the Elovich model is shown in Fig. 6a. As listed in Table 1, the experimental data of Cr(VI) adsorption on PACMC fit well with the Elovich model, where R^2 is 0.9998, which verifies the existence of chemisorption interaction here between adsorbent and the adsorbate [47].

In order to evaluate the intraparticle diffusion mechanism just at solid–liquid interface, we used the intraparticle diffusion model established by Weber and Morris [48]. As depicted in Fig. 6b, the plot of Q_t vs. $t^{1/2}$ exhibits a multilinear character, with the intraparticle diffusion model plot showing three linear components, the first corresponding to the migration of Cr(VI) ions from the aqueous medium to the surface interface of PACMC, a phase with a high rate due to the presence of a high number of active sites in the adsorbent. The second, slower phase shows the penetration of Cr(VI) ions through into inner surface of the PACMC and the rate of this phase is less than that of the first phase, attributed to the fact that Cr(VI) adsorption is controlled by pore diffusion [49]. The characteristic of the third stage curve is attributed to the gradual equilibrium of the adsorption [42]. The results show that none of the three lines cross thru the origin, demonstrating that intraparticle diffusion is not the sole rate-limiting step.

3.4. Adsorption isotherms

The non-linear fitting curves of the three models are depicted in Fig. 7a. Table 2 summarizes the relevant fitting parameters. The fitting data showed that the R^2 values of the three models were greater than 0.9. The chemical bonds in PACMC are not uniformly distributed, so various adsorptions occur simultaneously, so it is normal that the fitting parameter R^2 is higher for several models. The maximum adsorption capacity of PACMC was determined to be 52.804 mg·g^{-1}. In addition, when compared to the Freundlich and Langmuir isotherm models, the Temkin isotherm model seemed to be more suitable for describing the adsorption process with Cr(VI) by PACMC, and also the determination coefficient R^2 was greater than 0.98. Therefore, it was possible to postulate that the mechanism underlying Cr(VI) adsorption on PACMC can be explained by a monolayer-multilayer hybrid mechanism [50]. We can also note that the parameter $1 < n < 10$ obtained from the Freundlich isothermal adsorption model indicates that the adsorbent is favourable for Cr(VI) adsorption [51].

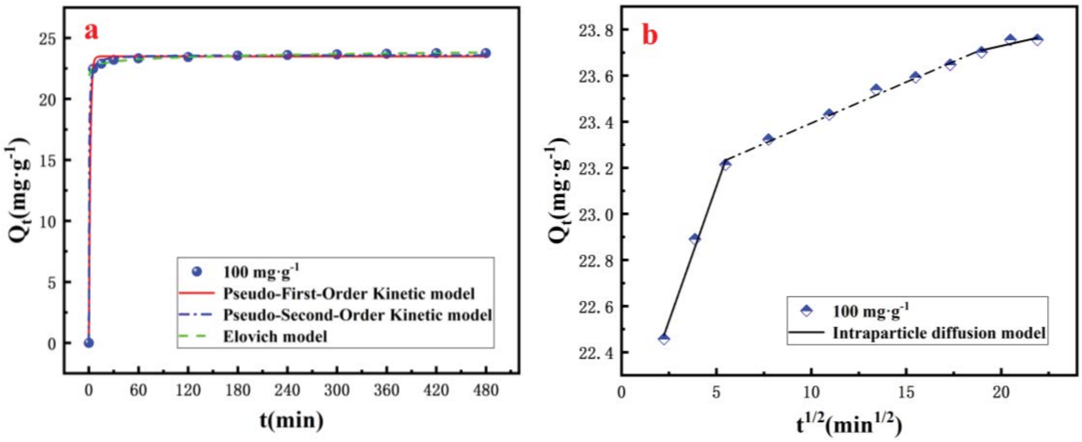

Fig. 6. (a) Pseudo-first-order, pseudo-second-order and Elovich non-linear models and (b) intraparticle diffusion model for the adsorption of Cr(VI) onto PACMC composite.

Table 1
Values of the kinetic parameters for Cr(VI) adsorption on the PACMC

C_0 (mg·L^{-1})	Pseudo-first-order model $Q_t = Q_e\left(1-\exp\left(-k_1 t\right)\right)$			Pseudo-second-order model $Q_t = \frac{Q_e^2 k_2 t}{1+Q_e k_2 t}$			Elovich model $Q_t = \frac{1}{\beta}\ln\left(\alpha\beta\right)+\frac{1}{\beta}\ln t$		
	k_1	$Q_{e.1}$	R^2	k_2	$Q_{e.2}$	R^2	α	β	R^2
100	0.625	23.485	0.9986	0.149	23.595	0.9995	22.161	0.265	0.9998
C_0 (mg·L^{-1})	Intraparticle diffusion model $Q_t = k_d t^{1/2} + C$								
	Initial phase			Second phase			Third phase		
	k_{d1}	C	R^2	k_{d2}	C	R^2	k_{d3}	C	R^2
100	0.234	21.951	0.9937	0.036	23.038	0.9936	0.019	23.357	0.7668

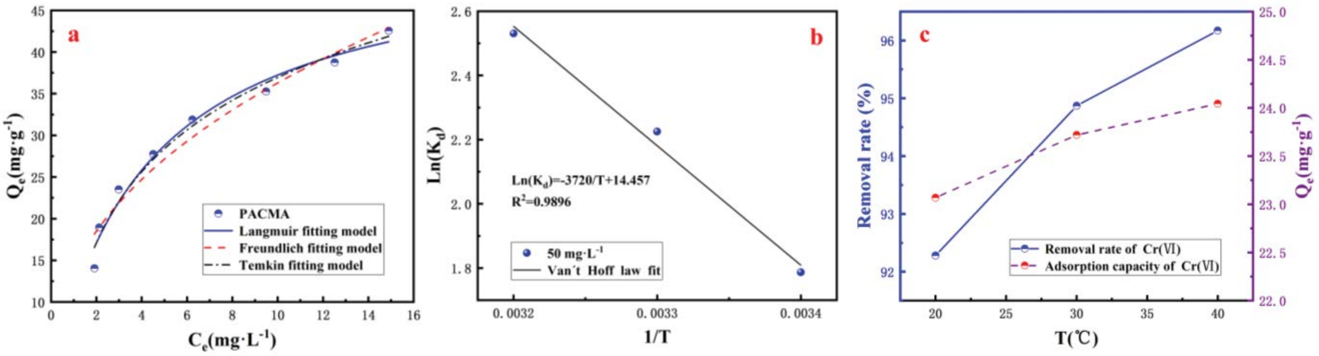

Fig. 7. (a) Non-linear fitting curves of Langmuir, Freundlich and Temkin isotherms for Cr(VI) adsorption onto PACMC composite, (b) van't Hoff plot for determining thermodynamic parameters and (c) effect of temperature on Cr(VI) adsorption by PACMC.

Table 2
Langmuir, Freundlich and Temkin constants for Cr(VI) adsorption onto PACMC composite

Model	Equation	R^2	Parameters	Parameter values
Langmuir	$Q_e = \frac{Q_{\max} K_L C_e}{1 + K_L C_e}$	0.979	$Q_{\max}$ K_L	52.804 0.239
Freundlich	$Q_e = K_F C_e^{1/n}$	0.958	K_F n	13.823 2.386
Temkin	$Q_e = B \ln K_T + B \ln C_e$	0.981	B K_T	12.342 1.997

Table 3
$\Delta G°$, $\Delta H°$, and $\Delta S°$ values for Cr(VI) adsorption on the PACMC composite

Adsorbent	$\Delta H°$ (kJ·mol^{-1})	$\Delta S°$ (J·mol^{-1}·K^{-1})	$\Delta G°$ (kJ·mol^{-1})		
			293	303	313
PACMC	30.93	120.19	–4.29	–5.48	–6.69

3.5. Adsorption thermodynamics

The intercept and slope of the lnK_d – 1/T plot (Fig. 7b) can be utilized to calculate $\Delta H°$ and $\Delta S°$, and the resulting thermodynamic parameters were shown in Table 3.

Fig. 7c exhibits an increasing trend of Cr(VI) absorption with temperature rose. As depicted in Table 3, the value of $\Delta H°$ is 30.93 kJ·mol^{-1}, which also confirms that the adsorption process with Cr(VI) ions onto PACMC is heat absorbing and the temperature rise is beneficial to the adsorption reaction. Generally, the value of $\Delta H°$ indicates the adsorption type where physical adsorption is characterized by $\Delta H°$ values between 2.1 and 20.9 kJ·mol^{-1} and the chemisorption is indicated by $\Delta H°$ values of 80–200 kJ·mol^{-1}, and when $\Delta H°$ between 20 and 80 kJ·mol^{-1}, chemical adsorption can be considered to gradually participate in the reaction [52]. According to the obtained $\Delta H°$ value (30.93 kJ·mol^{-1}), the removal process involved chemical adsorption. The measurement of $\Delta S°$ was 120.19 J·mol^{-1}·K^{-1} indicated that the disorder of solid–liquid contact surface was increasing during the adsorption process [49]. The value of $\Delta G°$ is negative at all experimental temperatures, demonstrating that the adsorption reaction was a spontaneous and feasible process [53]. At the same time, $\Delta G°$ decreases with increasing temperature, which further proves that Cr(VI) ion adsorption is more practical at higher temperatures [41].

3.6. Influence of co-existing ions

Various inorganic ions are frequently present in actual wastewater and natural water systems. These co-existing ions may compete for active adsorption sites during adsorption, which could ultimately affect the adsorption of Cr(VI). Fig. 8 depicted the effect of co-existing ions (Na^+, Ca^{2+}, SO_4^{2-}, Cl^-) on the adsorption of Cr(VI) on the composites. The results showed that Na^+, Cl^- and SO_4^{2-} ions had little effect on the removal of Cr(VI) ions, while Ca^{2+} had a negative effect. This phenomenon may be due to the competition between calcium ions and Cr(VI) for hydroxyl and carboxyl groups on the adsorbent surface, resulting in reduced adsorption capacity.

3.7. Proposed adsorption mechanism

Through the previously discussed results, it can be suggested the following mechanism for adsorption of Cr(VI) by PACMC composite (Fig. 9).

Adsorption of Cr(VI) on composites is related to the pore filling (physical adsorption): carbon-based materials possess a rich pore structure, and pore filling is the basic adsorption mechanism for the removal of contaminants

[54]. The process of diffusion and deposition of heavy metal ions in the pores of the adsorbent material, does not form chemical bonds, which is related to the pore size distribution of the adsorbent itself.

The electrostatic attraction between Cr(VI) and PACMC surface can also explain the adsorption mechanism. At pH below pH_{PZC} (<5.4), the PACMC surfaces become protonated promoting a strong electrostatic attraction between the anion ($HCrO_4^-$) and the adsorbent surface protonated functional group such as $–OH_2^+$ and $–COOH_2^+$. Adsorbents containing protonated functional groups adsorb Cr(VI) via electrostatic interactions:

$$R-OH_2^+ + HCrO_4^- \leftrightarrow \left(R-OH_2^+\right)\left(HCrO_4^-\right) \tag{I}$$

$$R-COOH_2^+ + HCrO_4^- \leftrightarrow \left(R-COOH_2^+\right)\left(HCrO_4^-\right) \tag{II}$$

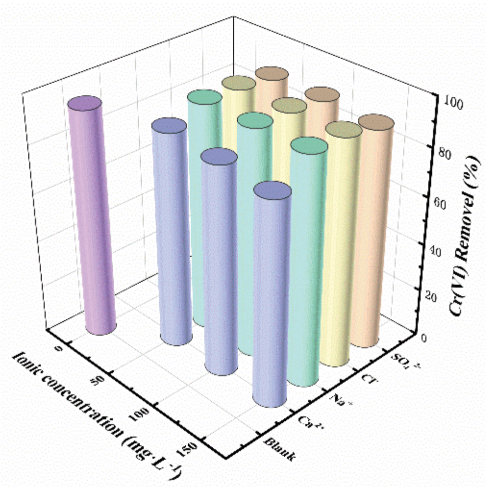

Fig. 8. Effect of co-existing ions on the removal of Cr(VI) by PACMC.

In addition, during the adsorption of Cr(VI) by PACMC, functional groups such as hydroxyl, carboxyl, and carbonyl played a key role in Cr(VI) adsorption, which can reduce Cr(VI) to Cr(III) under acidic conditions [55]. The PAC material itself contains hydroxyl and carboxyl groups. The composite material introduces HS, HS contains a large number of reducing functional groups (such as carboxyl, hydroxyl and carbonyl groups) that can be used as electron donors. In summary, carboxyl groups and hydroxyl groups in PACMC provide electrons, while Cr(VI) is strongly oxidizing, so the synthesized PACMC composite can effectively reduce Cr(VI) to Cr(III) under acidic conditions [56]. This can be expressed by the following reactions:

$$HCrO_4^- + 7H^+ + 3e^- = Cr^{3+} + 4H_2O \tag{III}$$

Additionally, we speculate that the –OH group of PACMC has a strong binding affinity for Cr(III), which may play a key role in the binding of Cr(III) on the adsorbent surface through the formation of $Cr(OH)^{3+}$ complexes. The hydroxyl complexation of the Cr(III) ion with PACMC can be expressed as:

$$R-OH + Cr^{3+} \rightarrow R-Cr\left(OH\right)^{3+} \tag{IV}$$

In summary, the removal of Cr(VI) by the composite adsorbent material PACMC is highly related to the solution pH, and factors such as electrostatic attraction, reduction, oxygen-containing functional group complexation and pore filling can all explain the removal mechanism of chromium ions.

3.8. Comparison of PACMC with other adsorbents

The performance of the PACMC for the adsorption of Cr(VI) was compared to that of other activated carbon composite adsorbents reported in the literature. Comparing

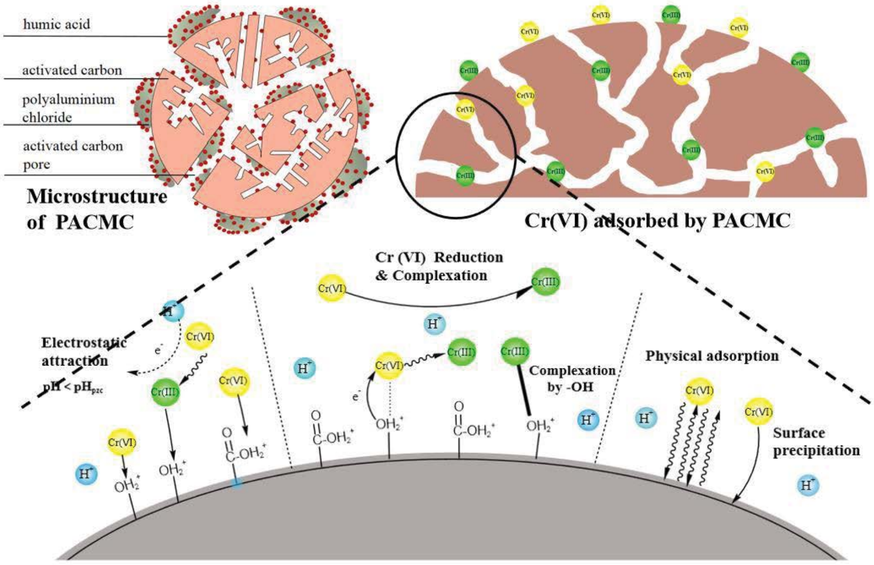

Fig. 9. Mechanism of adsorption of Cr(VI) by PACMC.

Table 4
Comparison with other activated carbon-based composite adsorbents

Adsorbent	Adsorption time (h)	$q_{\max}$ (mg/g)	Dosage (g/L)	pH	References
$ACDCS_{optimal}$	3	9.84	1.0	2	[57]
Ch-ACs	1	20.04	10.0	2	[58]
AC/nZVI	2	25.00	1.5	4	[24]
AC-PSR	72	8.929	3.0	4	[59]
CS/PVA/AC	6	109.89	0.8	2	[60]
AC-Fe_3O_4-NPs	1.5	15.24	1.0	3	[61]
Fe_2O_3@AC	10	32.10	2.0	5.6	[62]
PACMC	7	52.804	2.0	2	This study

diverse adsorbents can be challenging due to the different experimental conditions, hence in this research the maximum adsorption capacity ($q_{\max}$) was chosen as a parameter for comparison. According to Table 4, the PACMC performed well in the removal of Cr(VI) and had a greater maximum adsorption capacity than other activated carbon-based adsorbents. This also proved that the prepared composites is an effective, low-cost, and competitive adsorbent for Cr(VI) adsorption.

4. Conclusions

In this work, we had fabricated powdered activated carbon mixed humate and polyaluminum chloride functional composite (PACMC) by dissolved method, and the newly composite was employed as adsorbent for the removal of Cr(VI) from aqueous solution. The resultant composite had a high affinity for Cr(VI), and the maximum adsorption capacity was 52.804 mg/g, due to the abundant active functional group of HS.

Evaluate the effect of diverse parameters such as pH, adsorbent dose, initial concentration, and contact time on adsorption. Adsorption of Cr(VI) was more dependent on solution pH as the removal was found to be reasonably higher under low pH condition, and PACMC demonstrated the best adsorption affinity for Cr(VI) in aqueous solution at pH = 2. The high removal of 95.02% was obtained when Cr(VI) concentration was 50 mg/L, adsorbent dosage was 2 g/L, and pH value was 2.0 within 420 min operating time.

Kinetic investigation suggested the process of the removal of Cr(VI) was consistent with pseudo-second-order kinetics model($R^2 = 0.9995$) and Elovich model ($R^2 = 0.9998$), indicating that Cr(VI) was mainly adsorbed on the PACMC surface by chemical interaction. Intraparticle diffusion was not the only rate-limiting step in the Cr(VI) adsorption process. The Temkin model provided a good simulation of the adsorption procedure and suggested that hybrid monolayer-multilayer mechanism can account for the adsorption of Cr(VI) by PACMC ($R^2 = 0.981$). Moreover, thermodynamic investigations indicated that the sorption of Cr(VI) onto PACMC was an endothermic, spontaneous process in nature ($\Delta H°$= 30.93 kJ·mol^{-1}). Therefore, PACMC is an effective and economically viable adsorbent that can be utilized for the removal of Cr(VI) from aqueous solution.

References

[1] V.E. Pakade, N.T. Tavengwa, L.M. Madikizela, Recent advances in hexavalent chromium removal from aqueous solutions by adsorptive methods, RSC Adv., 9 (2019) 26142–26164.
[2] Y. wang, B. Wang, Q. Peng, X. Chen, Y. Huang, Adsorption of Cr(VI) by iron loaded porous carbon with high cycling properties, Mater. Lett., 274 (2020) 127988, doi: 10.1016/j.matlet.2020.127988.
[3] P. Sharma, S.P. Singh, S.K. Parakh, Y.W. Tong, Health hazards of hexavalent chromium (Cr(VI)) and its microbial reduction, Bioengineered, 13 (2022) 4923–4938.
[4] Z. Chen, B. Wei, S. Yang, Q. Li, L. Liu, S. Yu, T. Wen, B. Hu, J. Chen, X. Wang, Synthesis of PANI/AlOOH composite for Cr(VI) adsorption and reduction from aqueous solutions, ChemistrySelect, 4 (2019) 2352–2362.
[5] C. Sakulthaew, C. Chokejaroenrat, A. Poapolathep, T. Satapanajaru, S. Poapolathep, Hexavalent chromium adsorption from aqueous solution using carbon nano-onions (CNOs), Chemosphere, 184 (2017) 1168–1174.
[6] P. Bansal, R. Purwar, Polyacrylonitrile/clay nanofibrous nanocomposites for efficient adsorption of Cr(VI) ions, J. Polym. Res., 28 (2021) 1–19.
[7] A. Hsini, M. Benafqir, Y. Naciri, M. Laabd, A. Bouziani, M. Ez-zahery, R. Lakhmiri, N.E. Alem, A. Albourine, Synthesis of an arginine-functionalized polyaniline@FeOOH composite with high removal performance of hexavalent chromium ions from water: adsorption behavior, regeneration and process capability studies, Colloids Surf., A, 617 (2021) 126274, doi: 10.1016/j.colsurfa.2021.126274.
[8] D. Bagchi, Cytotoxicity and oxidative mechanisms of different forms of chromium, Toxicology, 180 (2002) 5–22.
[9] W. Wang, Q. Niu, G. Zeng, C. Zhang, D. Huang, B. Shao, C. Zhou, Y. Yang, Y. Liu, H. Guo, W. Xiong, L. Lei, S. Liu, H. Yi, S. Chen, X. Tang, 1D porous tubular g-C_3N_4 capture black phosphorus quantum dots as 1D/0D metal-free photocatalysts for oxytetracycline hydrochloride degradation and hexavalent chromium reduction, Appl. Catal., B, 273 (2020) 119051, doi: 10.1016/j.apcatb.2020.119051.
[10] J. Qiu, F. Liu, S. Cheng, L. Zong, C. Zhu, C. Ling, A. Li, Recyclable Nanocomposite of flowerlike MoS_2@hybrid acid-doped PANI immobilized on porous PAN nanofibers for the efficient removal of Cr(VI), ACS Sustainable Chem. Eng., 6 (2017) 447–456.
[11] WHO, Guidelines for Drinking-Water Quality, World Health Organization, 2004.
[12] A. Ramírez-Estrada, V.Y. Mena-Cervantes, J. Fuentes-García, J. Vazquez-Arenas, R. Palma-Goyes, A.I. Flores-Vela, R. Vazquez-Medina, R.H. Altamirano, Cr(III) removal from synthetic and real tanning effluents using an electro-precipitation method, J. Environ. Chem. Eng., 6 (2018) 1219–1225.
[13] G. Zolfaghari, M. Kargar, Nanofiltration and microfiltration for the removal of chromium, total dissolved solids, and sulfate from water, MethodsX, 6 (2019) 549–557.
[14] D. Pradhan, L.B. Sukla, M. Sawyer, P.K.S.M. Rahman, Recent bioreduction of hexavalent chromium in wastewater treatment: a review, J. Ind. Eng. Chem., 55 (2017) 1–20.
[15] C. Marcu, A. Balla, J.Z. Szűcs Balázs, C. Lar, Adsorption isotherms and thermodynamics for chromium(VI) using an anion exchange resin, Anal. Lett., 54 (2020) 1783–1793.
[16] D. Bekchanov, M. Mukhamediev, P. Lieberzeit, G. Babojonova, S. Botirov, Polyvinylchloride-based anion exchanger for efficient removal of chromium(VI) from aqueous solutions, Polym. Adv. Technol., 32 (2021) 3995–4004.
[17] M. Li, C. Song, Y. Wu, M. Wang, Z. Pan, Y. Sun, L. Meng, S. Han, L. Xu, L. Gan, Novel Z-scheme visible-light photocatalyst based on $CoFe_2O_4$/BiOBr/Graphene composites for organic dye degradation and Cr(VI) reduction, Appl. Surf. Sci., 478 (2019) 744–753.
[18] S. Prashanth, C. Subramaniam, V. Naren Bharatwaj, R. Aakash Kumar, K. Nithya, A. Sathish, *Chlorella sorokiniana* waste-based biomass for sorption of chromium ions from aqueous solution, Int. J. Environ. Sci. Technol., 19 (2021) 1247–1260.

[19] A. Bhatnagar, W. Hogland, M. Marques, M. Sillanpää, An overview of the modification methods of activated carbon for its water treatment applications, Chem. Eng. J., 219 (2013) 499–511.

[20] Y. Fang, K. Yang, Y. Zhang, C. Peng, A. Robledo-Cabrera, A. Lopez-Valdivieso, Highly surface activated carbon to remove Cr(VI) from aqueous solution with adsorbent recycling, Environ. Res., 197 (2021) 111151, doi: 10.1016/j.envres.2021.111151.

[21] E. Vunain, J.B. Njewa, T.T. Biswick, A.K. Ipadeola, Adsorption of chromium ions from tannery effluents onto activated carbon prepared from rice husk and potato peel by H_3PO_4 activation, Appl. Water Sci., 11 (2021) 1–14.

[22] Y. Matsui, S. Nakao, A. Sakamoto, T. Taniguchi, L. Pan, T. Matsushita, N. Shirasaki, Adsorption capacities of activated carbons for geosmin and 2-methylisoborneol vary with activated carbon particle size: effects of adsorbent and adsorbate characteristics, Water Res., 85 (2015) 95–102.

[23] B. Li, L. Zhang, W. Yin, S. Lv, P. Li, X. Zheng, J. Wu, Effective immobilization of hexavalent chromium from drinking water by nano-FeOOH coating activated carbon: adsorption and reduction, J. Environ. Manage., 277 (2021) 111386, doi: 10.1016/j.jenvman.2020.111386.

[24] S. Mortazavian, H. An, D. Chun, J. Moon, Activated carbon impregnated by zero-valent iron nanoparticles (AC/nZVI) optimized for simultaneous adsorption and reduction of aqueous hexavalent chromium: material characterizations and kinetic studies, Chem. Eng. J., 353 (2018) 781–795.

[25] Z.M. Magriotis, M.Z. Carvalho, P.F. de Sales, F.C. Alves, R.F. Resende, A.A. Saczk, Castor bean (*Ricinus communis* L.) presscake from biodiesel production: an efficient low-cost adsorbent for removal of textile dyes, J. Environ. Chem. Eng., 2 (2014) 1731–1740.

[26] P.E. Dim, L.S. Mustapha, M. Termtanun, J.O. Okafor, Adsorption of chromium(VI) and iron(III) ions onto acid-modified kaolinite: isotherm, kinetics and thermodynamics studies, Arabian J. Chem., 14 (2021) 103064, doi: 10.1016/j.arabjc.2021.103064.

[27] A. Essekri, A. Hsini, Y. Naciri, M. Laabd, Z. Ajmal, M. El Ouardi, A. Ait Addi, A. Albourine, Novel citric acid-functionalized brown algae with a high removal efficiency of crystal violet dye from colored wastewaters: insights into equilibrium, adsorption mechanism, and reusability, Int. J. Phytorem., 23 (2021) 336–346.

[28] V.C. Silva, M.E.B. Araujo, A.M. Rodrigues, M. Vitorino, J.M. Cartaxo, R.R. Menezes, G.A. Neves, Adsorption behavior of Crystal violet and Congo red dyes on heat-treated Brazilian Palygorskite: kinetic, isothermal and thermodynamic studies, Materials, 14 (2021) 5688, doi: 10.3390/ma14195688.

[29] X. Chi, L. Zeng, Y. Du, J. Huang, Y. Kang, J. Luo, Q. Zhang, Adsorption of levofloxacin on natural zeolite: effects of ammonia nitrogen and humic acid, Water Sci. Technol., 85 (2022) 2928–2944.

[30] C. Tejada-Tovar, Á. Villabona-Ortíz, Á.D. Gonzalez-Delgado, Adsorption of azo-anionic dyes in a solution using modified coconut (*Cocos nucifera*) mesocarp: kinetic and equilibrium study, Water, 13 (2021) 1382, doi: 10.3390/w13101382.

[31] S. Almohammadi, M. Mirzaei, Removal of copper(II) from aqueous solutions by adsorption onto granular activated carbon in the presence of competitor ions, Adv. Environ. Technol., 2 (2016) 85–94.

[32] L. Guan, H. Kang, W. Liu, D. Tian, Adsorption behavior of copper ions using crown ether-modified konjac glucomannan, Int. J. Biol. Macromol., 177 (2021) 48–57.

[33] S. Singh, S. Kaushal, J. Kaur, G. Kaur, S.K. Mittal, P.P. Singh, CaFu MOF as an efficient adsorbent for simultaneous removal of imidacloprid pesticide and cadmium ions from wastewater, Chemosphere, 272 (2021) 129648, doi: 10.1016/j.chemosphere.2021.129648.

[34] N. Aarab, A. Hsini, A. Essekri, M. Laabd, R. Lakhmiri, A. Albourine, Removal of an emerging pharmaceutical pollutant (metronidazole) using PPY-PANi copolymer: kinetics, equilibrium and DFT identification of adsorption mechanism, Groundwater Sustainable Dev., 11 (2020) 100416, doi: 10.1016/j.gsd.2020.100416.

[35] Y.J. Yang, B. Wang, X.J. Guo, C.W. Zou, X.D. Tan, Investigating adsorption performance of heavy metals onto humic acid from sludge using Fourier-transform infrared combined with two-dimensional correlation spectroscopy, Environ. Sci. Pollut. Res. Int., 26 (2019) 9842–9850.

[36] Z. Darvishi Chaghaganooj, N. Asasian-Kolur, S. Sharifian, M. Sillanpää, Ce and Mn/bio-waste-based activated carbon composite: characterization, phenol adsorption and regeneration, J. Environ. Chem. Eng., 9 (2021) 105788, doi: 10.1016/j.jece.2021.105788.

[37] M. Mobarak, R.A.M. Ali, M.K. Seliem, Chitosan/activated coal composite as an effective adsorbent for Mn(VII): modeling and interpretation of physicochemical parameters, Int. J. Biol. Macromol., 186 (2021) 750–758.

[38] M. Iqbal, A. Saeed, S.I. Zafar, FTIR spectrophotometry, kinetics and adsorption isotherms modeling, ion exchange, and EDX analysis for understanding the mechanism of Cd($^{2+}$) and Pb($^{2+}$) removal by mango peel waste, J. Hazard. Mater., 164 (2009) 161–171.

[39] Z. Guo, J. Zhang, Y. Kang, H. Liu, Rapid and efficient removal of Pb(II) from aqueous solutions using biomass-derived activated carbon with humic acid *in-situ* modification, Ecotoxicol. Environ. Saf., 145 (2017) 442–448.

[40] C. Jung, N. Phal, J. Oh, K.H. Chu, M. Jang, Y. Yoon, Removal of humic and tannic acids by adsorption–coagulation combined systems with activated biochar, J. Hazard. Mater., 300 (2015) 808–814.

[41] A. Hsini, Y. Naciri, M. Laabd, M. El Ouardi, Z. Ajmal, R. Lakhmiri, R. Boukherroub, A. Albourine, Synthesis and characterization of arginine-doped polyaniline/walnut shell hybrid composite with superior clean-up ability for chromium(VI) from aqueous media: equilibrium, reusability and process optimization, J. Mol. Liq., 316 (2020) 113832, doi: 10.1016/j.molliq.2020.113832.

[42] H.T. Ha, N.T. Huong, L.L. Dan, N.D. Tung, V.B. Trung, T.D. Minh, Removal of heavy metal ion using polymer-functionalized activated carbon: aspects of environmental economic and chemistry education, J. Anal. Methods Chem., 2020 (2020) 8887488, doi: 10.1155/2020/8887488.

[43] M.R. Lasheen, N.S. Ammar, H.S. Ibrahim, Adsorption/desorption of Cd(II), Cu(II) and Pb(II) using chemically modified orange peel: equilibrium and kinetic studies, Solid State Sci., 14 (2012) 202–210.

[44] J. Shang, Y. Guo, D. He, W. Qu, Y. Tang, L. Zhou, R. Zhu, A novel graphene oxide-dicationic ionic liquid composite for Cr(VI) adsorption from aqueous solutions, J. Hazard. Mater., 416 (2021) 125706, doi: 10.1016/j.jhazmat.2021.125706.

[45] M.K. Dinker, P.S. Kulkarni, Recent advances in silica-based materials for the removal of hexavalent chromium: a review, J. Chem. Eng. Data, 60 (2015) 2521–2540.

[46] M. Abbas, Z. Harrache, M. Trari, Mass-transfer processes in the adsorption of crystal violet by activated carbon derived from pomegranate peels: kinetics and thermodynamic studies, J. Eng. Fibers Fabr., 15 (2020), doi: 10.1177/1558925020919847.

[47] H.T. Dinh, N.T. Tran, D.X. Trinh, Investigation into the adsorption of Methylene blue and Methyl orange by UiO-66-NO_2 nanoparticles, J. Anal. Methods Chem., 2021 (2021) 5512174, doi: 10.1155/2021/5512174.

[48] S. Zhu, M. Asim Khan, F. Wang, Z. Bano, M. Xia, Rapid removal of toxic metals Cu^{2+} and Pb^{2+} by amino trimethylene phosphonic acid intercalated layered double hydroxide: a combined experimental and DFT study, Chem. Eng. J., 392 (2020) 123711, doi: 10.1016/j.cej.2019.123711.

[49] R. Das, S. Giri, A.M. Muliwa, A. Maity, High-performance Hg(II) removal using thiol-functionalized polypyrrole (PPy/MAA) composite and effective catalytic activity of Hg(II)-adsorbed waste material, ACS Sustainable Chem. Eng., 5 (2017) 7524–7536.

[50] H. Ouyang, S. Liu, D. Liu, Y. Wang, S. Xu, S. Pan, Fabrication of magnetic cobalt-nickel ferrite nanoparticles for the adsorption of methyl blue in aqueous solutions, Mater. Res. Express, 8 (2021) 105013, doi: 10.1088/2053-1591/ac3106.

[51] S. Azizkhani, S.A. Hussain, N. Abdullah, M.H.S. Ismail, A.W. Mohammad, Synthesis and application of functionalized graphene oxide-silica with chitosan for removal of Cd(II) from aqueous solution, J. Environ. Health Sci. Eng., 19 (2021) 491–502.

[52] M.M. Kamel, I.H. Alsohaimi, M.S. Alhumaimess, H.M.A. Hassan, M.S. Alshammari, M.Y. El-Sayed, A glassy polyvinyl alcohol/silica gel hybrid composite for safranin removal: adsorption, kinetic and thermodynamic studies, Res. Chem. Intermed., 47 (2020) 925–944.

[53] S.Z. Mohammadi, N. Mofidinasab, M.A. Karimi, F. Mosazadeh, Fast and efficient removal of Pb(II) ion and malachite green dye from wastewater by using magnetic activated carbon-cobalt nanoparticles, Water Sci. Technol., 82 (2020) 829–842.

[54] H. Ma, J. Yang, X. Gao, Z. Liu, X. Liu, Z. Xu, Removal of chromium(VI) from water by porous carbon derived from corn straw: influencing factors, regeneration and mechanism, J. Hazard. Mater., 369 (2019) 550–560.

[55] Y.J. Zhang, J.L. Ou, Z.K. Duan, Z.J. Xing, Y. Wang, Adsorption of Cr(VI) on bamboo bark-based activated carbon in the absence and presence of humic acid, Colloids Surf., A, 481 (2015) 108–116.

[56] B. Scaglia, F. Tambone, F. Adani, Cr(VI) reduction capability of humic acid extracted from the organic component of municipal solid waste, J. Environ. Sci., 25 (2013) 487–494.

[57] L. Li, Y. Li, Y. Liu, L. Ding, X. Jin, H. Lian, J. Zheng, Preparation of a novel activated carbon from cassava sludge for the high-efficiency adsorption of hexavalent chromium in potable water: adsorption performance and mechanism insight, Water, 13 (2021) 3602, doi: 10.3390/w13243602.

[58] F.H. Emamy, A. Bumajdad, J.P. Lukaszewicz, Adsorption of hexavalent chromium and divalent lead ions on the nitrogen-enriched chitosan-based activated carbon, Nanomaterials, 11 (2021) 1907, doi: 10.3390/nano11081907.

[59] S. Mortazavian, A. Saber, J. Hong, J.-H. Bae, D. Chun, N. Wong, D. Gerrity, J. Batista, K.J. Kim, J. Moon, Synthesis, characterization, and kinetic study of activated carbon modified by polysulfide rubber coating for aqueous hexavalent chromium removal, J. Ind. Eng. Chem., 69 (2019) 196–210.

[60] R. Nowruzi, M. Heydari, V. Javanbakht, Synthesis of a chitosan/polyvinyl alcohol/activate carbon biocomposite for removal of hexavalent chromium from aqueous solution, Int. J. Biol. Macromol., 147 (2020) 209–216.

[61] S. Afshin, Y. Rashtbari, M. Vosough, A. Dargahi, M. Fazlzadeh, A. Behzad, M. Yousefi, Application of Box–Behnken design for optimizing parameters of hexavalent chromium removal from aqueous solutions using Fe_3O_4 loaded on activated carbon prepared from alga: kinetics and equilibrium study, J. Water Process Eng., 42 (2021) 102113, doi: 10.1016/j.jwpe.2021.102113.

[62] B. Li, W. Yin, M. Xu, X. Tan, P. Li, J. Gu, P. Chiang, J. Wu, Facile modification of activated carbon with highly dispersed nano-sized α-Fe_2O_3 for enhanced removal of hexavalent chromium from aqueous solutions, Chemosphere, 224 (2019) 220–227.